ARMA 19-A-100

Determination of Horizontal Stresses in Anisotropic Formations Considering Tectonic Strain to Reduce Uncertainty in Wellbore Stability Analysis – Tampico-Misantla Basin Case Study

Morquecho-Robles, J. A.
Universidad Nacional Autónoma de México, Mexico City, Mexico
Velázquez-Cruz, D.
Tanis Tech Assist and Integral Services, Mexico City, Mexico
Espinosa-Castañeda, G.
Instituto Mexicano del Petróleo, Mexico City, Mexico

This paper was prepared for presentation at the 53rd US Rock Mechanics/Geomechanics Symposium held in New York, NY, USA, 23–26 June 2019. This paper was selected for presentation at the symposium by an ARMA Technical Program Committee based on a technical and critical review of the paper by a minimum of two technical reviewers. The material, as presented, does not necessarily reflect any position of ARMA, its officers, or members. Electronic reproduction, distribution, or storage of any part of this paper for commercial purposes without the written consent of ARMA is prohibited. Permission to reproduce in print is restricted to an abstract of not more than 200 words; illustrations may not be copied. The abstract must contain conspicuous acknowledgement of where and by whom the paper was presented.

ABSTRACT: This work presents a methodology that involves tectonic strain present in the wellbore to determine and analyze the magnitude of horizontal stresses in anisotropic formations through physical-mathematical models derived of Hooke's law. The methodology uses basic well log information, that is, horizontal stresses are determined from values of compressional velocity, shear velocity and clay content which is practical to use in the prediction. Furthermore, from ultrasonic measurements, an analysis of variation of mechanical properties was perform in three representative outcrop samples of Guayabal Formation. Classifying the mechanical behavior of this Formation as a medium with vertical transverse isotropy and taking it as the maximum anisotropy that can be presenting in determination of the profile of horizontal stresses in the wellbore. We estimated values for tectonic strain in Guayabal and Chicontepec Formations, and we determine the relationship between the maximum and minimum horizontal stresses. The profile of horizontal stresses was determine from sixteen wells where values obtained with the methodology were validate with Leak of Test, where it was observe that values estimated with the methodology are in the range of real values obtained from Leak of Test, hence, uncertainty was reduced.

1. INTRODUCCION

Wellbore instability is one of the main problems faced in drilling engineering, since they considerably increase the costs of operation and can even lead to abandonment of the wellbore. Estimates show that problems such as pack off and hole resistance, associated with wellbore instability, cause approximately 40% of all drilling downtime (Gala, 2010).

At present, determination of horizontal stresses is done by neglecting the strain associated with horizontal stresses, as well as, assuming that mechanical properties do not vary in different directions in which they are measured as shows in table 1 (Chenevert and Gatlin, 1964; Zhang, 2005; Zoback, 2007). Even when acoustic measurements in samples and well log data show a difference between the values measured in vertical and horizontal directions (Frydman, 2010; Franquet et al., 2012). Therefore, values of horizontal stresses obtained from models with the previous assumptions generate a bias comparing it with real magnitude. This uncertainty leads to problems with wellbore stability and cause economic losses during its construction (Gala, 2010).

Table 1. Proposed model for determinate horizontal stresses (modified from Zoback, 2017).

Author	Proposed Model
Hubbert and Willis (1957)	$\sigma_h = \frac{1+\sin\mu}{1-\sin\mu}\left(\sigma_v - P_p\right) + P_p$
Mathews and Kelly (1967)	$\sigma_h = K_i(z)\left(\sigma_v - P_p\right) + P_p$
Eaton (1969)	$\sigma_h = \left(\frac{\upsilon}{1-\upsilon}\right)\left(\sigma_v - P_p\right) + P_p$
Daines (1982)	$\sigma_h = \left(\frac{\upsilon}{1-\upsilon}\right)\left(\sigma_v - P_p\right) + P_p + \sigma_t$
Zoback and Healy (1984)	$\sigma_h = \left(\sqrt{1+\mu^2}+\mu\right)^{-2}\left(\sigma_v - P_p\right) + P_p$
Hoolbrook (1990)	$\sigma_h = (1-\varphi)\left(\sigma_v - P_p\right) + P_p$

In most sedimentary rocks, especially in shales, their properties vary widely in their different directions due to structure they present, that is, they are anisotropic (Ostadhassan, 2012). In case of shales, they exhibit

anisotropy in only one direction, because layers of stratification have a laminar structure and their mechanical properties are different from the axis perpendicular to the layer of stratification, giving it the character of transversely isotropic media (TI). Transverse isotropic media can be vertical or horizontal, depending on the direction of the axis parallel to isotropic plane as shown in figure 1 (Zhang, 2005; Frydman, 2010).

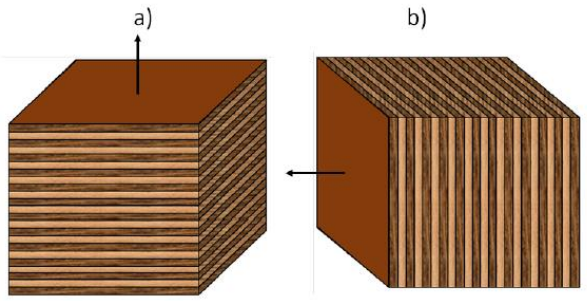

Fig. 1. Shale as a vertical transverse isotropic media (a) and horizontal transverse isotropic media (b).

In study of mechanical behavior, we consider that rocks follow the theory of linear elasticity. A medium follows the elasticity theory if strains associated with a load return to their original state when they stop applying the load, in rocks this elastic behavior is fulfilled when they are subjected to small strains (Amadei, 1983). Theory of linear elasticity follows what we call Hooke's law, which relates stress to strain, that is, strain is proportional to applied stress as shown in Eq. (1) (Jaeger et al., 2007).

$$\sigma_{ij} = C_{ijkl}\varepsilon_{kl} \tag{1}$$

The constant of proportionality that relates stress and strain depends mainly on constitutivity of material, that is, it depends on variation of the properties in different directions in which they are measured.

On the other hand, there are various tests that are commonly used to calibrate horizontal stresses. A direct test to determine the magnitude of the minimum horizontal stress is by means of leak of test (LOT). LOT are pressure tests performed during drilling and performed after the casing has been cemented. The value of this test is considered equal to the minimum horizontal stress measured at a certain depth, therefore, we can calibrate the stress profile (López et al., 2011; Moronkeji, 2014).

In present work, influence of anisotropy and tectonic strain of clay formations in the determination of horizontal stresses is evaluated. Consistently, a methodology was developed that involves anisotropy of material and tectonic strain in the prediction of horizontal stresses through physical-mathematical models derived from Hooke's law theory.

2. METHODOLOGY

Figure 2 shows the workflow to determine horizontal stresses assuming anisotropy where not only two elastic constants are determined, as in the isotropic case, but now it depends on the type of symmetry. In addition, to determine the magnitude of horizontal stresses, tectonic strain were considering.

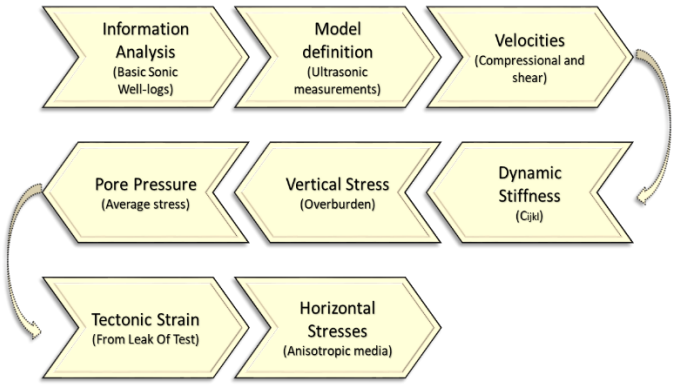

Fig. 2. Workflow to determine horizontal stresses assuming an anisotropic media.

2.1. Information Analysis

The first step to determine horizontal stresses is to identify study area where we can obtain representative samples (at the outcrop level) and we have basic well logs (sonic and resistivity).

It is important to have dipolar sonic well logs to correlate the constants measured in laboratory, however, these well logs are expensive and rarely used. Therefore, in this work, empirical models were developed and calibrated to obtain information that cannot be obtain directly from the well logs and can be used for any well in the Tampico-Misantla Basin. For developed and calibrated models, wells of different Fields within the Basin that have dipolar sonic well logs was use.

2.2. Model Definition

It is essential to obtain samples of Formation to study, since, when carrying out direct tests on samples we clarify the mechanical behavior of medium and, therefore, anisotropy that it presents. It is appropriate to obtain cubic samples and submit them to true triaxial tests, to represent the three main stresses, in order to obtain all stiffness coefficients. However, in some types of rock it is difficult to perform these tests. Another way to obtain the coefficients is from ultrasonic measurements on the different faces of the cubic sample and thus obtain the respective velocities, and subsequently, determine the coefficients using Eqs. (2) to (10) (Franquet et al., 2012).

$$C_{11} = \rho V_{p-x}^2 \tag{2}$$

$$C_{22} = \rho V_{p-y}^2 \tag{3}$$

$$C_{33} = \rho V_{p-z}^2 \tag{4}$$

$$C_{44} = \rho V_{s-yz}^2 \quad (5)$$

$$C_{55} = \rho V_{s-xz}^2 \quad (6)$$

$$C_{66} = \rho V_{s-xy}^2 \quad (7)$$

$$C_{12} = \sqrt{(2\rho V_{p-xy45}^2 - C_{66} - \frac{C_{22}}{2} - \frac{C_{11}}{2})^2 - \frac{1}{4}(C_{22} - C_{11})^2} - C_{66} \quad (8)$$

$$C_{13} = \sqrt{(2\rho V_{p-xz45}^2 - C_{55} - \frac{C_{11}}{2} - \frac{C_{33}}{2})^2 - \frac{1}{4}(C_{11} - C_{33})^2} - C_{55} \quad (9)$$

$$C_{12} = \sqrt{(2\rho V_{p-yz45}^2 - C_{44} - \frac{C_{22}}{2} - \frac{C_{33}}{2})^2 - \frac{1}{4}(C_{22} - C_{33})^2} - C_{44} \quad (10)$$

2.3. Velocities Determination

From basic well logs the compressional velocity (V_p) is determined from reciprocal of compressional transit time (DTC) obtained from well logs through Eq. (11).

$$V_p = \left(\frac{1}{DTC}\right) * a \quad (11)$$

Sonic well logs are very expensive and they are rarely used, therefore empirical models are used to determine shear velocity (V_s). The models most used are those presented by Greenberg and Castagna (1992). They showed that there is a relationship between compressional and shear velocities, developing linear correlations for different lithologies, as shows in Eqs. (12) to (15), such as shale, sand and dolomite; for limestone they found a second degree polynomial relation that adjusts better than linear regression.

Shale: $$V_s = 0.862V_p - 1.172 \quad (12)$$

Sand: $$V_s = 0.804V_p - 0.856 \quad (13)$$

Dolomite: $$V_s = 0.578V_p - 0.078 \quad (14)$$

Limestone: $$V_s = -0.055V_p^2 + 1.017V_p - 1.03 \quad (15)$$

Greenberg and Castagna models were obtain from clean formations, but the formations vary in clay content (V_{sh}), hence, these models can cause poor predictions of shear velocity (Fig. 3a).

For this reason, a model was determined which involves clay content and compressional velocity to determinate shear velocity. First step was to perform a statistical analysis to be able to define behavior patterns and verify the existence of linearity, homoscedasticity, independence and normality, to subsequently perform multiple regression.

In multiple linear regression we use more than one explanatory variable; this will offer us the advantage of using more information in the construction of the model and, consequently, making estimates with better precision. As in simple linear regression, it is considered that values of dependent variable $f(x_1, x_2, \dots, x_n)$ have been generated by a linear combination of values of one or more explanatory variables and a random term as shows in Eq. (16) (Uriel et al., 2002).

$$f(x_1, x_2, \dots, x_n) = b_0 + b_1x_1 + b_2x_2 + \cdots + b_nx_n \quad (16)$$

Its graphical representation is no longer in a Cartesian plane (x, y), as in a simple linear regression. In this case, it is now represented in a three-dimensional coordinate system (x_1, x_2, y) due to we have two independent variables and one dependent. Table 2 shows descriptive statistics of compressional velocity, shear velocity and clay content data from wells of different Fields within the Basin that have dipolar sonic well logs.

Table 2. Descriptive statistics of V_p, V_s and V_{sh} data from wells of different Fields within the Tampico-Misantla Basin.

Descriptive Statistics					
Variable	***Count***	***Mean***	***Standard Deviation***	***Minimum Value***	***Maximum Value***
V_p (m/s)	35,931	3469.53	2529.76	2301.54	6136.25
V_s (m/s)	35,931	1721.82	2103.17	806.62	4179.44
V_{sh}	35,931	0.39	0.22	0.00	0.999

After carry out descriptive statistics, multiple linear regression was performed and one model was obtained from shear velocity data which is dependent variable, compressional velocity and clay content data, which are independent variables as it is shown in Eq. (17).

$$V_s = 0.8037V_p + 385.6931V_{sh} - 1219.1988 \quad (17)$$

The coefficient correlation is $R^2 = 0.9222$. Which means that model estimated is acceptable to determine shear velocity (Fig. 3b).

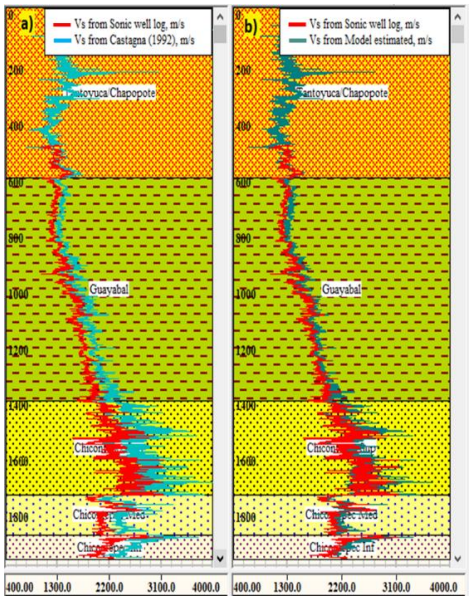

Fig. 3. Sensitivity analysis of shear velocity determined from Greenberg and Castagna models (a) and from model estimated by multiple regression (b) with respect to measurements obtained from sonic well logs.

2.4. *Dynamic Stiffness*

Determining stiffness matrix for anisotropic media from well logs is complicated, even when dipolar sonic well logs are available, due to lack of necessary information to obtain six stiffness coefficients (in case of a VTI media).

Thomsen (1986) introduced anisotropic parameters for VTI media in order to describe behavior of velocities in different directions. The epsilon parameter (ε) is used to perceive the difference of compressional waves that travel horizontally and vertically as shows in Eq. (18). Similarly, the gamma parameter (γ) is used, but in this case, to perceive the difference of shear waves as shows in Eq. (19). Finally, the delta parameter (δ) is a combination of elastic constants that denotes the difference in velocities at angles of 0, 45 and 90 degrees, it shows in Eq. (20).

$$\varepsilon = \frac{C_{11}-C_{33}}{2C_{33}} \tag{18}$$

$$\gamma = \frac{C_{66}-C_{44}}{2C_{44}} \tag{19}$$

$$\delta = \frac{(C_{13}+C_{44})^2-(C_{33}-C_{44})^2}{2C_{33}(C_{33}-C_{44})} \tag{20}$$

In methodology, elastic coefficients for VTI media are determined from density, wave propagation velocities (Vp and Vs) and anisotropic parameters ε and γ. Assuming that we can only determine the compressional velocity from sonic well logs and that we can determine the shear velocity from model estimated by linear regression, as shows in Eqs. (21) and (22), we can only determine the stiffness coefficients C_{33} and C_{44}.

$$C_{33} = \rho V_p^2 \tag{21}$$

$$C_{44} = \rho V_s^2 \tag{22}$$

Determining coefficients C_{11} and C_{66}, models developed by Thomsen (1986) are used in Eqs. (18) and (19), where we solve C_{11} and C_{66} having now two models based on anisotropic parameters as shows in Eqs. (23) and (24).

$$C_{11} = C_{33}(2\varepsilon + 1) \tag{23}$$

$$C_{66} = C_{44}(2\gamma + 1) \tag{24}$$

Now, using the ANNIE approximation developed by Schoenberg et al. (1996), it is assumed that $\delta = 0$. Then, replacing and algebraically solving from Eq. (20), we have the Eq. (25), so stiffness coefficient C_{13} is determined.

$$C_{13} = C_{33} - 2C_{44} \tag{25}$$

The coefficient C_{12} depends on C_{11} and C_{66}, and is determined with Eq. (26).

$$C_{12} = C_{11} - 2C_{66} \tag{26}$$

We observe that to determine C_{11} and C_{66} using Eqs. (23) and (24) we need to determine anisotropic parameters. Yongy Li (2006) developed two models to determine anisotropic parameters from compressional velocity, shear velocity and clay content. Tests carried out in his study were based on data from rock samples in laboratory, therefore, in order to be able to use them in our study, there was a need to calibrate the models to be able to apply them from well logs.

Calibrating Li models, wells of different Fields within the Tampico-Misantla Basin were use obtaining three stiffness constants from dipolar sonic well logs using Eqs. (27) and (29).

$$C_{33} = \rho\left(\frac{1}{DTC}\right)^2 \tag{27}$$

$$C_{44} = \rho\left(\frac{1}{DTS}\right)^2 \tag{28}$$

$$C_{66} = \rho\left(\frac{1}{DTST}\right)^2 \tag{29}$$

The three remaining coefficients are determined from the ANNIE approximation, where it is assume that $\delta = 0$ and C_{12} equal to C_{13} (Schoenberg et al., 1996).

$$C_{12} = C_{13} \tag{30}$$

$$C_{13} = C_{33} - 2C_{44} \tag{31}$$

$$C_{12} = C_{11} - 2C_{66} \tag{32}$$

After of determinate the six stiffness coefficients from dipolar sonic well logs and ANNIE approximation, a scatter plot made to observe the relationship between velocities and anisotropic parameters. The epsilon parameter plotted versus compressional velocity because epsilon perceives the difference of compressional waves in their horizontal and vertical directions. The gamma parameter plotted versus shear velocity because gamma perceives the difference of shear waves in their horizontal and vertical directions. Both graphs, at the same time, based on clay content as shown in figure 4. In both figures, it is observed that when increasing the clay content the anisotropy increases and velocity decrease. Three critical points defined; the point 1 is considering the case of 100% porosity, called critical porosity. Points 2 and 3 considered 100% clay and 0% clay, respectively.

Assuming that the fluid in pores is water, we have that for point 1 the anisotropy is equal to zero and the compressional and shear velocities is equal to the water velocity ($V_{p-w} = 1500\ ^m/_s$, $V_{s-w} = 0\ ^m/_s$). In point 2, it exhibits the greatest anisotropy when we have a formation with 100% clay, therefore, the velocity corresponds to velocity of clay ($V_{p-cl} = 3400\ ^m/_s$, $V_{s-cl} = 1800\ ^m/_s$). In point 3, as in point 1, there is no anisotropy in the medium and it is displayed for a formation with 0% clay, then the velocity corresponds to the velocity of the quartz ($V_{p-qtz} = 6050\ ^m/_s$, $V_{s-qtz} = 4090\ ^m/_s$).

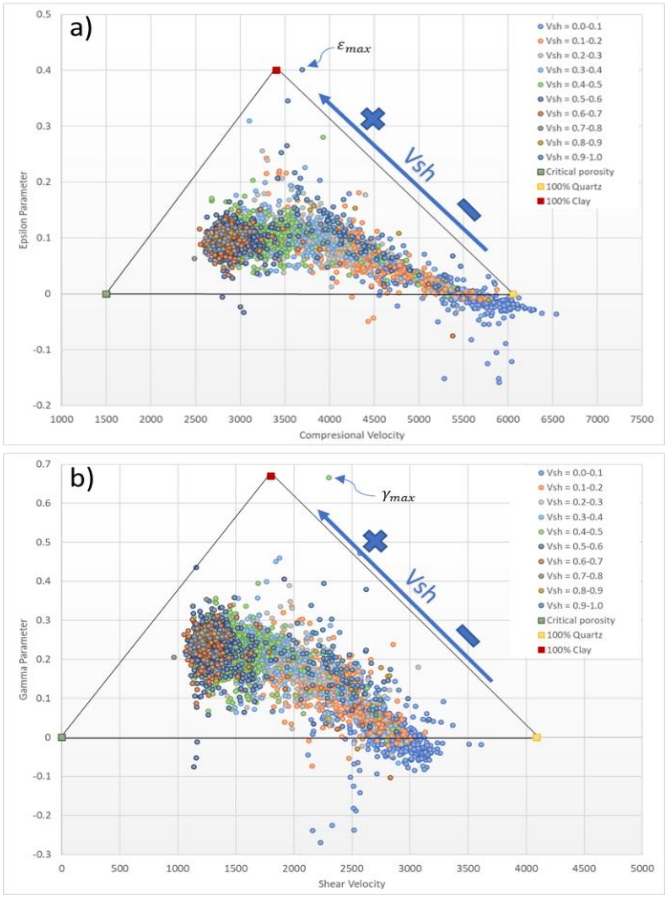

Fig. 4. Scatter plot anisotropic parameters versus velocities, considering content clay.

Using line's equation, in point-slope form:

$$y - y_1 = m(x - x_1) \tag{33}$$

Now, in terms of anisotropic parameters and velocities:

$$\varepsilon - \varepsilon_1 = m(V_p - V_{p1}) \tag{34}$$

$$\gamma - \gamma_1 = m(V_s - V_{s1}) \tag{35}$$

Where ε_1 and V_{p1} come into point 1 of scatter plot (a) in figure 4. In the same way, $\gamma_1$and V_{s1} come into point 1 of scatter plot (b) in figure 4. In both cases, anisotropic parameters are equal to zero and velocities are equal to water velocity.

On the other hand, we determinate the slope using the Eqs. (36) and (37):

$$m = \frac{\Delta y}{\Delta x} = \frac{\varepsilon_i V_{sh} - \varepsilon_1 V_{sh}}{V_{pi} - V_{p1}} \tag{36}$$

$$m = \frac{\Delta y}{\Delta x} = \frac{\gamma_i V_{sh} - \gamma_1 V_{sh}}{V_{si} - V_{s1}} \tag{37}$$

In Eqs. (36) and (37) Δy is function of the anisotropic parameters that, at the same time, depend of content clay. For example, 0% clay ε_i and γ_i are zero, 100% clay ε_i and γ_i obtain maximum value. In our study $\varepsilon_i = \varepsilon_{max} = 0.41$ and $\gamma_i = \gamma_{max} = 0.68$. In case for Δx is function of velocities where V_{pi} and V_{si} depend both of characteristic values of shale and sand velocities and content clay. When we have 0% clay the characteristic velocity is of a sand, otherwise, if we have 100% clay the characteristic velocity is of a shale. Now, we can express the slope with Eqs. (38) and (39).

$$m = \frac{\varepsilon_{max} V_{sh}}{V_{p\_qtz} - V_{sh}(V_{p\_qtz} - V_{p\_cl}) - V_{p\_w}} \tag{38}$$

$$m = \frac{\gamma_{max} V_{sh}}{V_{p\_qtz} - V_{sh}(V_{p\_qtz} - V_{p\_cl})} \tag{39}$$

Replacing Eqs. (38) and (39) in Eqs. (34) and (35), we have the models calibrated to determine the parameters anisotropic from sonic well logs as shows in Eqs. (40) and (41).

$$\varepsilon = \frac{\varepsilon_{max} V_{sh} (V_p - V_{p\_w})}{V_{p\_qtz} - V_{sh}(V_{p\_qtz} - V_{p\_cl}) - V_{p\_w}} \tag{40}$$

$$\gamma = \frac{\gamma_{max} V_{sh} V_s}{V_{s\_qtz} - V_{sh}(V_{s\_qtz} - V_{s\_cl})} \tag{41}$$

2.5. *Vertical Stress*

Fundamental variable to determine vertical or overburden stress is the density. During sedimentation process, an accumulated weight is generate on sediments, causing the fluids to be compacted and expelled from the porous medium, which leads to a reduction in porosity, and consequently, an increase in density with depth.

In the case where the fluids cannot get out of the porous space, the porosity is not reduce with the depth due to the force exerted by fluids on pore causing that pressure to increase. Therefore, the pressure and porosity will be abnormally high, causing an abnormal decrease in the density of the rock. Then, when measuring the density with well logs, it will be affect by the fluids contained in the pores, the quality of the hole and the presence of abnormal pressures.

Determining the vertical or overburden stress, the following model is used (Velázquez et al., 2017).

$$\sigma_v = \frac{\sum_{n=1}^{n} (\rho_o + k Z_i^m)[Z_i - Z_{i-1}]}{Z_i} \tag{42}$$

The model uses an exponential model to normalize the density, where ρ_o is the bulk density at mudline, m is constant of compaction and varies between 0.3 and 0.6, k is declination parameter equal to 0.01. These values were adjust for wells of northern Mexican basins.

2.6. *Pore Pressure*

Pore pressure can be predict in formations that follow the theory of compaction (commonly shales), in other types of formations, pore pressure has to be measure. If pore pressure is a compartmentalized pressure envelope, then its pressure indicators behave as a "divergent area" (Velázquez et al., 2017).

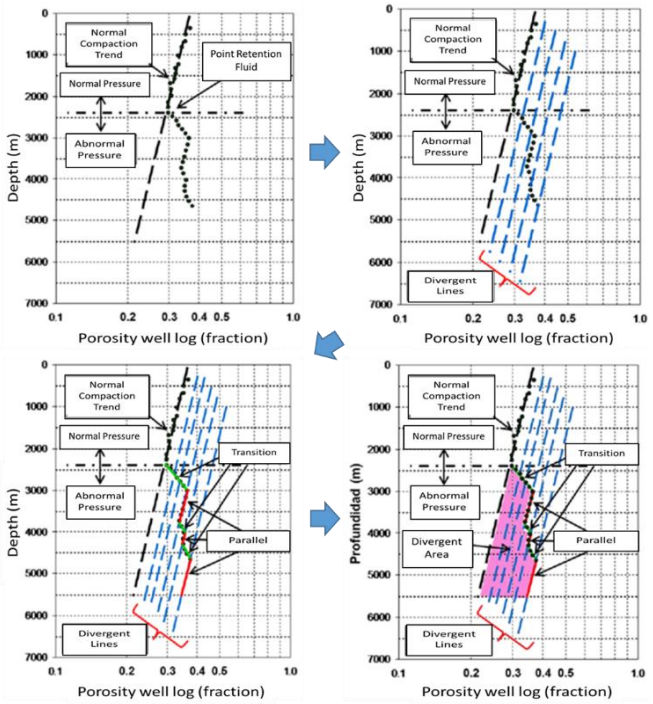

Fig. 5. Divergence method consists in generating compaction trends parallels to normal compaction trend to determine area divergent (modified from Velázquez et al., 2017).

Determining the pore pressure, the divergence method was use, which consists in generating compaction trends parallels to normal compaction trend in resistivity and sonic well logs, in order to generate a divergent area as shows in figure 5.

Once this area is defined, any method based on well logs can be used to calculate the pore pressure. For this work, the expressions of Eaton (1975) were used to calculate pore pressure from the resistivity and sonic well logs.

$$P_P = OBG - (OBG - P_P)\left(\frac{R_o}{R_n}\right)^{\alpha} \quad (43)$$

$$P_P = OBG - (OBG - P_P)\left(\frac{DT_n}{DT_o}\right)^{\alpha} \quad (44)$$

2.7. *Tectonic Strain*

Tectonic strains was estimated from wells of different Fields within the Tampico-Misantla Basin that have LOT. We also consider the anisotropy in the estimate of tectonic strains.

Considering that, strain associate to maximum horizontal stress is "n" times bigger that strain associate to minimum horizontal stress. From statistical analysis, we obtained the magnitudes of tectonic strains for Guayabal and Chicontepec formations as shows in Table 3.

Table 3. Relationship between tectonic strain associated to maximum and minimum horizontal stresses.

Guayabal			***Chicontepec***		
ε_h	ε_H	$\varepsilon_H/\varepsilon_h$	ε_h	ε_H	$\varepsilon_H/\varepsilon_h$
3.80 E-05	6.49 E-05	**1.72**	-7.12 E-05	-1.29 E-04	**1.84**

We observe that tectonic strains from Guayabal Formation is positive, meaning that wellbore is enlarges. Conversely, Chicontepec Formation has negative tectonic strains due to wellbore is reduced. Figure 6 shows behavior previously described for a well of the Basin.

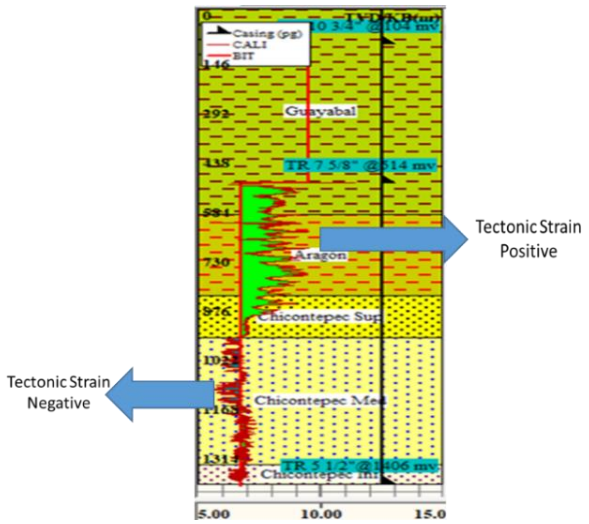

Fig. 6. Convention of signs for tectonic strains.

2.8. *Horizontal stresses*

Starting from Hooke's law, the general case consider to stiffness tensor of fourth-order with 81 coefficients, because it is assumed that there is no symmetry in stress and strain tensors (Fjaer et al., 2008). In others words, when exchanging the sub-index leads to altering the sign of tensor ($C_{ijkl} \neq C_{jikl}$ and $C_{ijkl} \neq C_{jilk}$).

In practical applications, It is possible simplify the stiffness tensor. Considering that, there is symmetry in stress and strain tensors, Voigt index notation, strain energy density conditions and molecular structure of materials.

Considering an orthorhombic structure we have a medium with anisotropy in three orthogonal directions, called orthotropic media with nine stiffness coefficients, the matrix representative is showed in Eq. (45) where we can observed that elements below of diagonal main are symmetric.

$$\begin{pmatrix}\sigma_1\\ \sigma_2\\ \sigma_3\\ \sigma_4\\ \sigma_5\\ \sigma_6\end{pmatrix} = \begin{pmatrix} C_{11} & C_{12} & C_{13} & 0 & 0 & 0\\ C_{12} & C_{22} & C_{23} & 0 & 0 & 0\\ C_{13} & C_{23} & C_{33} & 0 & 0 & 0\\ 0 & 0 & 0 & C_{44} & 0 & 0\\ 0 & 0 & 0 & 0 & C_{55} & 0\\ 0 & 0 & 0 & 0 & 0 & C_{66}\end{pmatrix}\begin{pmatrix}\varepsilon_1\\ \varepsilon_2\\ \varepsilon_3\\ \varepsilon_4\\ \varepsilon_5\\ \varepsilon_6\end{pmatrix} \quad (45)$$

Considering that stresses are in terms of effective vertical and horizontal stresses, transforming them in an equation system and solved we have horizontal stress models for orthotropic media as shows in Eqs. (46) and (47).

$$\sigma_h = \alpha_i P_p + \frac{C_{13}}{C_{33}}(\sigma_v - \alpha P_p) + \left(C_{11} - \frac{C_{13}^2}{C_{33}}\right)\varepsilon_h + \left(C_{12} - \frac{C_{13}C_{23}}{C_{33}}\right)\varepsilon_H \quad (46)$$

$$\sigma_H = \alpha_i P_p + \frac{C_{23}}{C_{33}}(\sigma_v - \alpha P_p) + \left(C_{12} - \frac{C_{13}C_{23}}{C_{33}}\right)\varepsilon_h + \left(C_{11} - \frac{C_{13}^2}{C_{33}}\right)\varepsilon_H \quad (47)$$

From horizontal stresses models for an orthotropic media, we can simplify the models according to molecular structure. In this work, the maximum anisotropy found in wells of Tampico-Misantla Basin was a special case of orthotropic media, called VTI Media. Models for VTI media consider that $C_{23} \approx C_{13}$ and $C_{44} \approx C_{55}$, due to propagation of velocities in the horizontal plane are approximately equal associated to laminar structure. Therefore, horizontal stresses models for a VTI media are showed in Eqs. (48) and (49).

$$\sigma_h = \alpha_i P_p + \frac{C_{13}}{C_{33}}(\sigma_v - \alpha P_p) + \left(C_{11} - \frac{C_{13}^2}{C_{33}}\right)\varepsilon_h + \left(C_{12} - \frac{C_{13}^2}{C_{33}}\right)\varepsilon_H \quad (48)$$

$$\sigma_H = \alpha_i P_p + \frac{C_{23}}{C_{33}}(\sigma_v - \alpha P_p) + \left(C_{12} - \frac{C_{13}^2}{C_{33}}\right)\varepsilon_h + \left(C_{11} - \frac{C_{13}^2}{C_{33}}\right)\varepsilon_H \quad (49)$$

3. APPLICATION AND RESULTS

The methodology was applied for wells where the Guayabal Formation is on surface, this Formation represents a medium with high clay content. It is located outcropping to 12 km west of Potrero Del Llano in Veracruz, Mexico as mentioned by Lopez Ramos (1979). This area was defined to obtain representative cubic samples of outcrop of the Guayabal Formation (figure 7), whose purpose is to perform ultrasonic measurements on the samples and determine the anisotropy according to the structure of shales (Orthotropic, VTI, Isotropic).

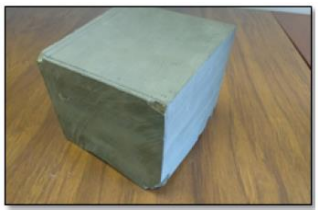

Fig. 7. Cubic sample of outcrop of the Guayabal Formation.

Figure 8 shows the mechanical behavior of the Guayabal Formation on three samples of outcrop. We observed that stiffness coefficients C_{13} and C_{44} are approximately equal to C_{23} and C_{66}, respectively. Mechanical behavior that presents the Guayabal Formation is similar to VTI media, due to laminar structure that we observed on the samples. Thus, we can used the models for a VTI media to determinate horizontal stresses.

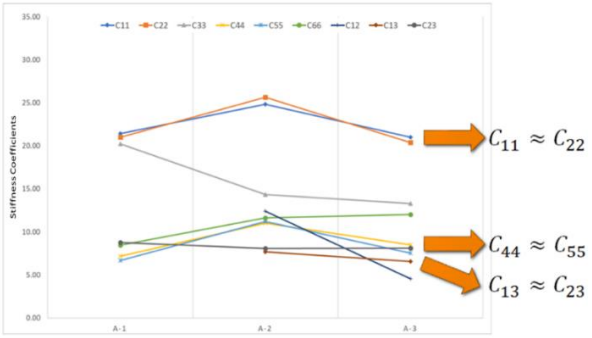

Fig. 7. Mechanical behavior of the Guayabal Formation shows similar behavior to VTI media.

Once the mechanical behavior is defined and identify what kind of anisotropy of the formation, we quantify the anisotropy using anisotropic parameters ε and γ. The Guayabal Formation has bigger magnitudes than other formations and due to content clay is greater in Guayabal than other formations in wellbore as shows in figure 8.

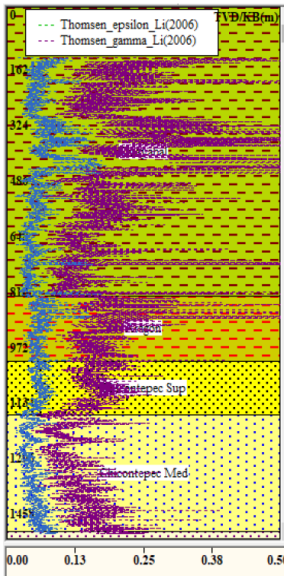

Fig. 8. Anisotropic parameters determined for a wellbore in the study area. We observe that anisotropy is greater for Guayabal than other formations in the wellbore.

Through a statistical analysis of sixteen wells where Guayabal Formation crops, we obtain an average value of the anisotropic parameters for Guayabal Formation using Eqs. (40) and (41).

Table 4. Anisotropic parameters for Guayabal Formation.

Guayabal Formation	
ε	γ
0.05 (±0.025)	0.16 (±0.089)

From velocities (compresional and shear) and anisotropic parameters data, stiffness coefficients was determined for 16 wells, using Eqs. (21) to (26). We obtained an average value of each coefficient for Guayabal Formation, and therefore, a characteristic matrix as shows in Eq. (50).

$$C_{ijkl} = \begin{pmatrix} 15.22 & 9.40 & 9.56 & 0 & 0 & 0 \\ 9.40 & 15.22 & 9.56 & 0 & 0 & 0 \\ 9.56 & 9.56 & 13.80 & 0 & 0 & 0 \\ 0 & 0 & 0 & 2.12 & 0 & 0 \\ 0 & 0 & 0 & 0 & 2.12 & 0 \\ 0 & 0 & 0 & 0 & 0 & 2.91 \end{pmatrix} \quad (50)$$

Figure 9 is noted that stiffness coefficients obtain from ultrasonic measurements is greater than stiffness coefficients obtain from sonic well logs. The reason is due to frequency, hence, to high frequency we have high stiffness, and on the contrary, to low frequency we have low stiffness. It is important to validate what information we intend to work, since we cannot use it to determine average values of stiffness coefficients if we mix seismic, well logs and ultrasonic measurements data.

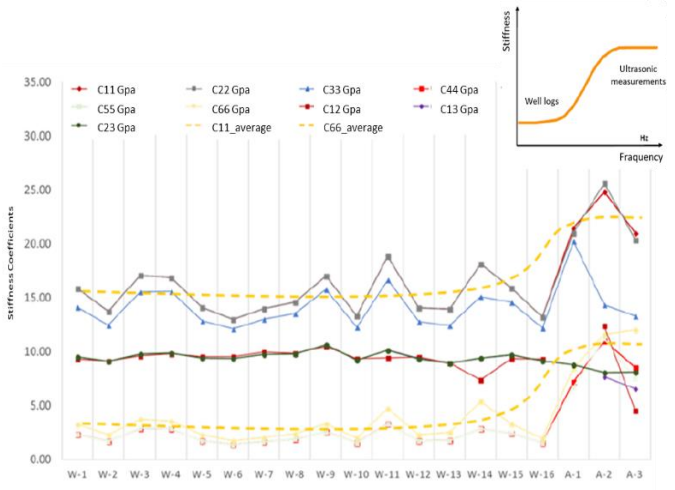

Fig. 9. Stiffness coefficients determined for sixteen wells and three outcrop samples and influence of frequency.

By models that define a VTI medium, Magnitude of horizontal stresses of Guayabal Formation was determined as shows in Eqs. (48) and (49). At the same time, using the World Stress Map we obtained the orientation of the *in-situ* stresses.

We can define that the state of horizontal stresses for the Guayabal Formation is:

- $\sigma_H = 0.0197\ MPa/m\ \ (2.01\ g/cc)$ with direction $N\ 2°\ S$
- $\sigma_h = 0.0191\ MPa/m\ \ (1.95\ g/cc)$ with direction $N\ 92°\ S$

Relationship between maximum and minimum horizontal stresses is in the range 1.03 to 1.05 in the Guayabal Formation.

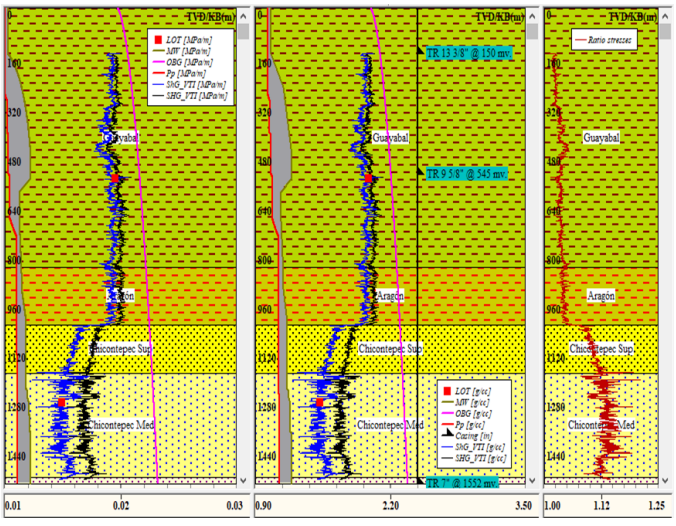

Fig. 10. Determination of a safe mud window (track 1 in MPa/m and track 2 in g/cc) and ratio stresses (track 3) for an analysis of wellbore stability where is considering anisotropy and tectonic strain.

Finally, a sensitivity analysis was made between the Eaton model and those used in this methodology that consider anisotropy and tectonic strains, where we appreciate that the uncertainty is reduced when considering the constitutivity of the material. Figure 11 is observed that the uncertainty is reduced if we considered the anisotropy and tectonic strain in determination of horizontal stresses, hence, the uncertainty in wellbore stability analysis is reduced.

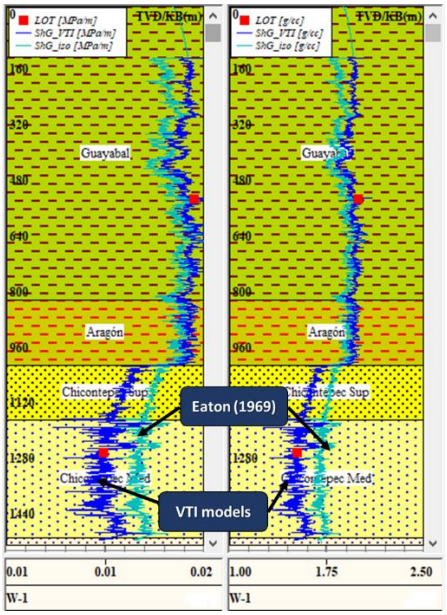

Fig. 11. Sensitivity analysis between Eaton model (turquoise) and VTI model (blue) regarding to LOT values.

4. DISCUSSIONS

From velocity values obtained in representative samples of the Guayabal Formation, it has been possible to identify the type of anisotropy present. We classify the mechanical behavior of shale as a vertical transverse isotropic medium, corroborating the investigations of several authors such as Chenevert and Gatlin (1964), Zhang (2005), Frydman (2010) and Franquet et al. (2012) regarding the type of anisotropy present in rocks with high clay content. For the case of the anisotropic parameters, in the scatter plots of Figure 4 presented above, it was observed that the anisotropy is affected by clay content, that is, if the clay content in a formation increases the anisotropy increases.

Errors in the estimation of horizontal stresses result from biases or trends in the input variables. Due to the sequential nature of the evaluations, errors in the estimation occur in several stages and propagate through the process to estimate the horizontal stresses. In addition, the conventional models mentioned in table 1 to determine the horizontal stresses do not consider the variation of mechanical properties and tectonic strain, increasing the uncertainty considerably. Despite this uncertainty, these models are still used and the main reason is that the stiffness coefficients were almost impossible to obtain to determine the horizontal stresses considering anisotropy and tectonic strain.

NOMENGLATURE

$a = Conversion\ factor, [ft/\mu s]\ to\ [m/s]\ equal\ to\ 304{,}800$

$C_{ijkl} = fourth - order\ stiffness\ tensor, GPa$

$C_{ij} = Voigt\ index\ stiffness\ tensor, GPa$

$C_{11} = Compression\ stiffness\ in\ x\ direction, GPa$

$C_{22} = Compression\ stiffness\ in\ y\ direction, GPa$

$C_{33} = Compression\ stiffness\ in\ z\ direction, GPa$

$C_{44} = Shear\ stiffness\ in\ xz\ plane, GPa$

$C_{55} = Shear\ stiffness\ in\ yz\ plane, GPa$

$C_{66} = Shear\ stiffness\ in\ xy\ plane, GPa$

$C_{12} = non - diagonal\ stiffness\ term\ in\ xy, GPa$

$C_{13} = non - diagonal\ stiffness\ term\ in\ xz, GPa$

$C_{23} = non - diagonal\ stiffness\ term\ in\ yz, GPa$

$DTC = Compressional\ slowness, \mu s/ft$

$DT_n = Normal\ compaction\ trend\ slowness, \mu s/ft$

$DT_o = Compressional\ slowness\ of\ well\ log, \mu s/ft$

$m = Slope\ of\ curve, unitless$

$OBG = Overburden\ stress, MPa$

$P_p = Pore\ pressure, MPa$

$R_n = Normal\ compaction\ trend\ resistivity, ohmm$

$R_o = Resistivity\ of\ well\ logs, ohmm$

$V_p = Compressional\ velocity, m/s$

$V_s = Shear\ velocity, m/s$

$V_{p-x} = Compressional\ velocity\ in\ x\ direction, m/s$

$V_{p-y} = Compressional\ velocity\ in\ y\ direction, m/s$

$V_{p-z} = Compressional\ velocity\ in\ z\ direction, m/s$

$V_{s-yz} = Shear\ velocity\ in\ yz\ plane\ vertical, m/s$

$V_{s-xz} = Shear\ velocity\ in\ xz\ plane\ vertical, m/s$

$V_{s-xy} = Shear\ velocity\ in\ xy\ plane\ horizontal, m/s$

$V_{p-xy45} = Compressional\ velocity\ at\ 45^o\ in\ xy\ plane\ , m/s$

$V_{p-xz45} = Compressional\ velocity\ at\ 45^o\ in\ xz\ plane\ , m/s$

$V_{p-yz45} = Compressional\ velocity\ at\ 45^o\ in\ yz\ plane\ , m/s$

$V_{p\_w} = Compressional\ velocity\ of\ water, m/s$

$V_{p\_qtz} = Compressional\ velocity\ of\ quartz, m/s$

$V_{p\_cl} = Compressional\ velocity\ of\ clay, m/s$

$V_{s\_w} = Shear\ velocity\ of\ water, m/s$

$V_{s\_qtz} = Shear\ velocity\ of\ quartz, m/s$

$V_{s\_cl} = Shear\ velocity\ of\ clay, m/s$

$V_{sh} = Content\ clay, unitless$

$\alpha = Eaton's\ exponent, unitless$

$\alpha_i = Poroelastic\ Biot's\ coefficient, unitless$

$\gamma = Gamma\ anisotropic\ parameter, unitless$

$\varepsilon = Epsilon\ anisotropic\ parameter, unitless$

$\varepsilon_h = Tectonic\ strain\ in\ minimum\ direction, unitless$

$\varepsilon_H = Tectonic\ strain\ in\ maximum\ direction, unitless$

$\rho_o = bulk\ density\ at\ mudline, g/cc$

$\sigma_v = Vertical\ stress, MPa$

$\sigma_h = Minimum\ horizontal\ stress, MPa$

$\sigma_H = Maximum\ horizontal\ stress, MPa$

ACKNOWLEDGMENT

The authors are grateful to Instituto Mexicano del Petróleo for support to develop and giving the authorization to publish this paper

REFERENCES

1. Amadei, B. 1983. *Rock anisotropy and the theory of stress measurements*. Lecture Notes in Engineering, Vol. 2, pp. 482. Berlin, Heidelberg: Springer-Verlag.
2. Chenevert M. E. & Gatlin C. 1964. *Mechanical Anisotropies of Laminated Sedimentary Rocks*. Society of Petroleum Engineers, Vol. 5, pp. 11. Presented at 39th Annual Fall Meeting of SPE in Houston, Tx., Oct.11- 14.
3. Eaton, B. A., 1975. *The equation for geopressure prediction from well logs*. Society of Petroleum Engineers of AIME, paper SPE 5544.
4. Fjaer, E., et al. 2008. *Petroleum related rock mechanics*. Elsevier Science, 2nd Edition, Vol. 53, pp. 514. Printed and bound in Hungary.
5. Franquet, J. A., & Rodríguez, E. F. 2012. *Orthotropic Horizontal Stress Characterization from Logging and Core Derived Acoustic Anisotropies*. American Rock Mechanics Association, pp. 9. In 46th US Rock Mechanics/Geomechanics Symposium, Chicago, Illinois.
6. Frydman, M. 2010. *Determinations of the Dynamic Elastic Constants of a Transverse Isotropic Rock Based on Borehole Dipole Sonic Anisotropy in Deviated Wells*. IBP2304 10. Rio Oil & Gas - Expo and Conference 2010, pp. 10. Rio de Janeiro, Brasil.
7. Gala, D. M. et al. 2010. *Drilling Hazard Mitigation Technologies Key in Eliminating Non-Productive Time in Challenging Wells*. In SPE Oil and Gas India Conference and Exhibition pp. 18. Society of Petroleum Engineers. Mumbai, India.
8. Greenberg, M. L., & Castagna, J. P. 1992. *Shear-wave velocity estimation in porous rocks: theoretical formulation, preliminary verification and applications*. Geophysical prospecting, 40(2), 195-209. European Association of Geoscientists & Engineers. Houston, TX.
9. Jaeger, J. C., Cook, N. G., & Zimmerman, R. 2007. *Fundamentals of rock mechanics*. Wiley-Blackwell, 4 edition, pp. 488.

10. Li, Y. 2006. *An empirical method for estimation of anisotropic parameters in clastic rocks*. The Leading Edge, 25(6), 706-711. Paradigm Geophysical, Calgary, Alberta, Canada.

11. López-Ramos, E. 1979. *Geología de México, Tomo II*. 2nd. Edition, Mexico, D.F., pp. 454.

12. López-Solís et. al. 2011. *Análisis de pruebas de goteo extendidas para la determinación del gradiente de fractura y esfuerzo mínimo*. VII INGEPET 2011 (EXPL-2-DV-04-E), pp. 7. Mexico.

13. Moronkeji, Dee A., et al. 2014. *Anisotropic Stress Profiling and Tectonic Strain Calibration in a Tight Basement Formation*. ISRM Conference on Rock Mechanics for Natural Resources and Infrastructure-SBMR 2014, pp. 14. International Society for Rock Mechanics. Goiania, Brazil.

14. Ostadhassan, M., Zeng, Z., & Zamiran, S. 2012. *Geomechanical modeling of an anisotropic formation-Bakken case study*. In 46th US Rock Mechanics/Geomechanics Symposium, pp. 15. American Rock Mechanics Association. Chicago, Illinois.

15. Schoenberg M., Muir F. and Sayers C. 1996. *Introducing ANNIE: a simple three-parameter anisotropic velocity model for shales*. J. Seismic Explor., 5, 35-49.

16. Thomsen, L. 1986. *Weak elastic anisotropy*. Society of Exploration Geophysicists, 51(10), 1954-1966. Tulsa, USA.

17. Uriel, E., & Manzano, J. A. 2002. *Análisis multivariante aplicado*. Paraninfo Cengage Learning, Vol. 76, pp. 531. Madrid, Spain.

18. Velázquez Cruz, D., et al. 2017. *New Methodology for Pore Pressure Prediction Using Well Logs and Divergent Area*. Society of Petroleum Engineers. doi:10.2118/185557-MS. SPE Latin America and Caribbean Petroleum Engineering Conference, May 17-19. Buenos Aires, Argentina.

19. Zhang, J. 2005. *The Impact of Shale Properties on Wellbore Stability*. Dissertation, pp. 276. The University of Texas. Austin, Tx.

20. Zoback, Mark. D. 2007. *Reservoir Geomechanics*. Cambridge University Press, pp. 423.